Methods for sequential resonance assignment in solid, uniformly 13C, 15N labelled peptides: Quantification and application to antamanide

Author(s):
Detken, Andreas; Hardy, Edme H.; Ernst, Matthias; Kainosho, Masatsune; Kawakami, Toru; Aimoto, Saburo; Meier, Beat H.

Publication date:
2001

Permanent link:
https://doi.org/10.3929/ethz-b-000422779

Originally published in:
Journal of Biomolecular NMR 20(3), https://doi.org/10.1023/A:1011212100630

Journal of Biomolecular NMR, **20:** 203–221, 2001.
KLUWER/ESCOM

Methods for sequential resonance assignment in solid, uniformly ^{13}C, ^{15}N labelled peptides: Quantification and application to antamanide

Andreas Detken[a], Edme H. Hardy[a], Matthias Ernst[a], Masatsune Kainosho[b], Toru Kawakami[c], Saburo Aimoto[c] & Beat H. Meier[a,*]
[a]*Laboratory of Physical Chemistry, ETH Hönggerberg, CH-8093 Zürich, Switzerland;* [b]*CREST, Japan Science and Technology Corporation, Tokyo Metropolitan University, 1-1 Minami-ohsawa, Hachioji, Tokyo 192-0397, Japan;* [c]*Institute for Protein Research, Osaka University, 3-2 Yamadaoka, Suita, Osaka 565-0871, Japan*

Received 21 February 2001; Accepted 16 April 2001

Key words: adiabatic, antamanide, assignment, cross polarization, DREAM, MAS, polarization transfer, solid-state NMR, TOBSY, TOSSY

Abstract

The application of adiabatic polarization-transfer experiments to resonance assignment in solid, uniformly ^{13}C-^{15}N-labelled polypeptides is demonstrated for the cyclic decapeptide antamanide. A homonuclear correlation experiment employing the DREAM sequence for adiabatic dipolar transfer yields a complete assignment of the C^{α} and aliphatic side-chain ^{13}C resonances to amino acid types. The same information can be obtained from a TOBSY experiment using the recently introduced $P9^{l}_{12}$ TOBSY sequence, which employs the J couplings as a transfer mechanism. A comparison of the two methods is presented. Except for some aromatic phenylalanine resonances, a complete sequence-specific assignment of the ^{13}C and ^{15}N resonances in antamanide is achieved by a series of selective or broadband adiabatic triple-resonance experiments. Heteronuclear transfer by adiabatic-passage Hartmann–Hahn cross polarization is combined with adiabatic homonuclear transfer by the DREAM and rotational-resonance tickling sequences into two- and three-dimensional experiments. The performance of these experiments is evaluated quantitatively.

Introduction

Magic-angle spinning (MAS) solid-state NMR is an established method to measure distances and torsion angles in selectively labelled biomolecules. Because selective labelling is laborious and expensive, high-resolution solid-state NMR methods for structure determination in uniformly labelled biomolecules are highly desirable.

Recent progress in NMR technology and techniques as well as advances in sample-preparation techniques made it possible to obtain ^{13}C and ^{15}N linewidths below 100 Hz in magnetic fields of 14–19 Tesla for powdered uniformly labelled samples of peptides and small proteins (McDermott et al., 2000; Pauli et al., 2000). This resolution should be sufficient to resolve in multidimensional NMR experiments the resonances of considerably larger peptides than demonstrated so far. Because the achievable resolution of the ^{1}H resonances is still very limited, usually resonance assignments in the solid state have to be based on the connectivities of ^{13}C and ^{15}N nuclei. In the last few years, a large number of techniques have been developed that can be potentially useful for resonance assignment in solid, uniformly ^{13}C and/or ^{15}N labelled biomolecules under MAS (for an overview see Griffin (1998)).

This paper discusses the *sequential* resonance assignment of the ^{13}C and ^{15}N resonances, which is a prerequisite for atomistic structure determination by NMR. All spectra are recorded under MAS. At finite frequencies, MAS leads to a center line at approximately the isotropic chemical-shift position and

*To whom correspondence should be addressed. E-mail: Beat.Meier@nmr.phys.chem.ethz.ch

sidebands spaced by the spinning frequency. For increasing MAS frequency, the intensity of the sidebands drops drastically (the second moment of the entire sideband family stays constant) at the benefit of the centerband, which moves to the exact isotropic chemical-shift position (Meier and Earl, 1987; Nakai and McDowell, 1992). To avoid significant loss of signal intensity to sidebands, the MAS frequency must be at least comparable to or preferably higher than the anisotropy of the chemical-shift tensors. The required MAS frequency, therefore, scales linearly with the static magnetic field. Furthermore, the MAS frequency must be chosen carefully to avoid accidental matching of rotational-resonance conditions. It is, therefore, most convenient to use a MAS frequency that is larger than the total width of the spectrum. For ^{13}C spectroscopy in a 14 Tesla field, this requires MAS frequencies exceeding 25 kHz. Such MAS frequencies can be easily reached in modern MAS probes with small-diameter (e.g. 2.5 mm) rotors. They require, however, polarization-transfer pulse sequences designed for these MAS frequencies. This aspect shall be emphasized in this paper.

In solid-state NMR, assignments are often done using ^{13}C-^{13}C and ^{15}N-^{13}C dipolar (through-space) correlations (Hong, 1999; Pauli et al., 2001). Recently, solid-state NMR techniques have been developed which use the ^{13}C-^{13}C scalar (through-bond) J-couplings (Baldus and Meier, 1996; Hardy et al., 2001). Both classes of techniques will be compared. While the TOBSY (total through-bond correlation spectroscopy) experiment must be performed as a 'sudden' experiment, through-space correlations can be established using adiabatic polarization-transfer methods (Hediger et al., 1994, 1995; Zhang et al., 1994; Baldus et al., 1996; Verel et al., 1997, 1998), where the density operator stays aligned with the Hamiltonian at all times of the mixing period. Adiabatic methods offer a number of advantages over sudden methods, the most important ones, for biological samples, being a high theoretical transfer efficiency of up to 100% and a reduced susceptibility to spectrometer missettings and instabilities. Heteronuclear transfer (especially ^{1}H-^{13}C and ^{15}N-^{13}C) by adiabatic-passage Hartmann–Hahn cross polarization (APHH CP) has already been used in several solid-state NMR studies. Here we aim at designing experiments that offer adiabatic performance in *all* steps of homo- and heteronuclear polarization transfer and which may be applied at MAS frequencies above 25 kHz.

The system under study is the cyclic decapeptide antamanide, whose primary sequence (Wieland, 1968) is shown in Figure 1. In nature, antamanide is found in small quantities in the poisonous mushroom *Amanita phalloides* ('green deathcap'). It exhibits antitoxic activity against the phallotoxins contained in the same mushroom by blocking the entrance of these toxins through the cytoplasmic membrane and by competitively blocking their receptors (Wieland and Faulstich, 1978). Antamanide has been studied by X-ray crystallography (Karle et al., 1979) and liquid-state NMR (Kessler et al., 1989a, b). Recently, a solid-state NMR study of antamanide has been published in which a full assignment of the ^{13}C resonances was given (Straus et al., 1997). Here, we will report a significantly improved spectral resolution of the ^{13}C resonances and an assignment of the ^{15}N resonances.

In this paper, much emphasis will be put on the optimization of the polarization transfer that leads to the assignment. In particular, we will address the question of efficiency of the polarization transfer which directly expresses itself in the signal-to-noise ratio and is particularly important if the methods are scaled up for applying them to larger peptides and proteins.

The paper is organized as follows: in the Materials and methods section, the preparation of the antamanide sample is described, and the experimental parameters of the employed NMR techniques are given. Subsequently, the pulse sequences that were used for the assignment are briefly described. In the Results and discussion section, the assignment of the ^{13}C and ^{15}N antamanide resonances by two-dimensional correlation experiments is outlined. Particularities of the pulse sequences are discussed in some detail, with an emphasis on the application to biomolecules. Specifically, the experimental efficiency of the involved polarization-transfer steps is quantified. Finally, extensions of the employed techniques to three dimensions are discussed.

Materials and methods

Sample preparation

Fully ^{13}C, ^{15}N-labelled antamanide was synthesized by a Boc solid-phase method, starting from Boc-^{13}C, ^{15}N-labelled Pro-OCH$_2$-C$_6$H$_4$-CH$_2$-CONH-CH$_2$-resin (Pro: 0.37 mequiv/g resin, 344 mg). A peptide chain was assembled on a resin by the *in situ* neutralization method (Schnolzer et al., 1992). The obtained Boc-Pro-Ala-Phe-Phe-Pro-Pro-Phe-Phe-Val-

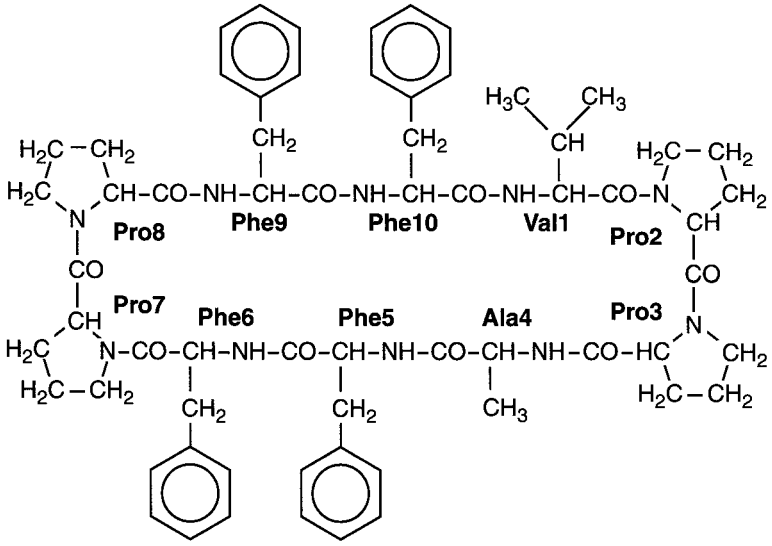

Figure 1. Sketch of the antamanide molecule. The secondary structure is dominated by the two hairpin turns in the two *cis* Pro-Pro peptide bonds.

Pro-OCH_2-C_6H_4-CH_2CONH-CH_2-resin (470 mg) was treated with anhydrous HF (Sakakibara et al., 1967). After evaporation of the HF, the product was dissolved in aqueous acetonitrile and the peptide solution was freeze-dried to a powder (165 mg). An aliquot of this powder (146 mg, ca. 0.1 mmol), 1-hydroxy-7-azabenzotriazole (41 mg, 0.3 mmol), and diisopropylethylamine (87 µl, 0.5 mmol) were dissolved in 1-methyl-2-pyrrolidinone (NMP) (10 ml). One-tenth of this peptide solution and one-tenth of an NMP solution (1 ml) containing *O*-(7-azabenzotriazol-1-yl)-1,1,3,3-tetramethyluronium hexafluorophosphate (76 mg, 0.2 mmol) were simultaneously added to NMP (20 ml) at 40-min intervals, with constant stirring. After completion of the addition, the reaction mixture was further stirred overnight. The product was isolated from the solution by a Cosmosil 5C18 AR column (Nacalai Tesque, Kyoto) using aqueous acetonitrile containing 0.1% trifluoroacetic acid as an eluent to give the product, ^{13}C, ^{15}N-labelled cyclo-(Pro-Ala-Phe-Phe-Pro-Pro-Phe-Phe-Val-Pro) (95 mg, 0.079 mmol, 63% yield based on the proline content in the starting resin); MS (matrix-assisted laser desorption ionization-time of flight MS): m/z 1219.8. Calculated for $[M+H]^+$: 1221.8 (exact).

The solution was lyophilized, and batches of 12 mg of the peptide were recrystallized from a methanol/water mixture. The ^{13}C and ^{15}N linewidths in the MAS NMR spectra depended critically on the preparation of the sample, especially on the rate of evaporation and the final water content. While the principal route of preparation is the same as in a previous study (Straus et al., 1997), details of the crystallization procedures such as humidity and evaporation rate were optimized to achieve a significantly improved structural homogeneity. The narrowest lines were obtained from a sample prepared by slowly evaporating the solvent from a solution of 12 mg peptide in 250 µl of a 7:3 methanol/water mixture over a period of 4 days in a controlled relative humidity of 76% (maintained by a concentrated solution of NaCl in H_2O), resulting in needle-like crystals. The substance (10 mg, corresponding to about 7–8 µmol, depending on the unknown water content) was carefully crushed into a fine powder and filled into a standard 2.5 mm o.d. rotor. The sample was stable without noticeable changes in its NMR spectrum over a period of more than 6 months.

NMR data collection

Experiments were performed at a B_0 field of 14.09 T on a Bruker DMX-600 widebore spectrometer equipped with a Bruker 2.5 mm triple-resonance MAS probe. The MAS frequency was actively stabilized to within ±5 Hz. To counteract sample heating due to spinning (Grimmer et al., 1997; Langer et al., 1999), the sample was cooled to a nominal temperature of 278 K. During the detection and evolution periods, high-power proton decoupling was applied using the TPPM decoupling scheme (Bennett et al., 1995). A proton field strength of $\omega_1^H/2\pi = 150$ kHz, a phase-

modulation angle of $\pm 15°$ and a pulse length of 3.1 μs were used. All ^{13}C chemical shifts are referenced to external TMS; for the ^{15}N chemical shifts, indirect referencing to external TMS was employed with a Ξ ratio of 0.101329144 (Live et al., 1984), yielding ^{15}N shifts relative to liquid ammonia.

^{1}H-^{13}C/^{15}N cross polarization

In all experiments, APHH CP (Hediger et al., 1994, 1995) from the protons was used to generate the initial ^{15}N or ^{13}C polarization. We introduced the following modification to the standard method: The initial 90° pulse that is commonly applied for creating transverse proton magnetization was replaced by an adiabatic half-passage (AHP) sweep. The particular amplitude and frequency modulation scheme for the AHP sweep was chosen as (Garwood and Ke, 1991; Hwang et al., 1998):

$$\omega_1(t) = \omega_1^{\max} \tanh(\zeta t/T) \tag{1}$$

and

$$\Delta\omega(t) = \Delta\omega_{\max} \frac{\tan(\kappa \cdot [1 - t/T])}{\tan(\kappa)} \quad \text{for } 0 < t < T \tag{2}$$

where $\omega_1(t)$ is the rf-field amplitude in angular frequency units and $\Delta\omega(t)$ is the frequency offset from the approximate center of the proton spectrum. The adjustable parameters were chosen as $\omega_1^{\max}/2\pi = 80$ kHz, $\Delta\omega_{\max}/2\pi = 300$ kHz, $\zeta = 10$, and $\tan(\kappa) = 20$. The total sweep length was $T = 50$ μs. A detailed discussion of AHP sweeps in conjunction with CP will be given elsewhere. This modification leads to a gain in total ^{13}C intensity, compared to APHH CP with an initial 90° pulse, amounting to ca. 9% for our antamanide sample and spectrometer configuration. This gain can be rationalized by considering the inhomogeneity of the rf field sensed by the protons. For a nominal 90° proton pulse, different parts of the sample experience different flip angles, leading to incomplete alignment of the proton magnetization with the following spin-lock field during CP. This problem is circumvented by the AHP sweep, which leads to proton magnetizations that are aligned with the CP spin-lock field.

^{15}N-^{13}C cross polarization

Nitrogen-carbon polarization transfer was achieved by APHH CP (Baldus et al., 1996) at a MAS frequency of 20 kHz. The ^{15}N spin-lock field was chosen as $\omega_1^{\mathrm{N}}/2\pi = 30$ kHz, avoiding the rotary-resonance conditions at 20 and 40 kHz. On the ^{13}C channel, a tangential modulation of the rf field amplitude of the following form was used (Hediger et al., 1994, 1995):

$$\omega_1^{\mathrm{C}}(t) = \omega_1^{\mathrm{HH}} \pm \beta \cdot \tan\left(\alpha \cdot \left[\frac{\tau}{2} - t\right]\right) \quad \text{for } 0 \le t \le \tau, \tag{3}$$

where

$$\alpha = \frac{2}{\tau} \arctan\left(\frac{\Delta}{\beta}\right). \tag{4}$$

Here $\omega_1^{\mathrm{HH}}/2\pi = (\omega_1^{\mathrm{N}} + \omega_r)/2\pi = 50$ kHz is the rf field on the ^{13}C channel at the $f = 1$ Hartmann–Hahn matching condition. A sweep length of $\tau = 8$ ms was used. The transfer efficiency was found to depend strongly on the choice of the shape parameters Δ and β. The best results were achieved with $\Delta/2\pi = 8$ kHz and $\beta/2\pi = 2$ kHz. Selectivity to either the C^{α} or the C' regions depended on the transmitter offset of the ^{13}C channel and the direction of the applied shape ('up' or 'down', depending on the sign in Equation 3). Empirically we found that for transfer to the C^{α} region irradiation at 53 ppm with an 'up' shape (positive sign) proved optimal; for transfer to the C' region, irradiation at 185 ppm with a 'down' shape (negative sign) gave the best results. During CP, homonuclear Lee–Goldburg decoupling (Lee and Goldburg, 1965; Baldus et al., 1996; Baldus, 1996) was applied to the protons with an rf-field strength of $\omega_1^{\mathrm{H}}/2\pi = 150$ kHz.

^{13}C-^{13}C through-space polarization transfer

Homonuclear transfer via the dipolar interactions was induced using the DREAM scheme (Verel et al., 1998, 2001) and the rotational resonance tickling (R^2T) scheme (Takegoshi et al., 1995, 1997; Costa et al., 1997). The DREAM sweep is schematically depicted in Figure 2a. During the sweep, the variation of the rf-field strength followed a tangential modulation of the same general form as in Equation 3, where ω_1^{HH} is to be replaced by the rf-field strength at the HORROR condition, $\omega_r/2$. A 'down' shape was applied (negative sign in Equation 3). The MAS frequency was set to $\omega_r/2\pi = 30$ kHz in the homonuclear two-dimensional correlation experiments and to 20 kHz in the heteronuclear correlation experiments. The length of the DREAM sweep was $\tau = 7$ ms, the shape parameters were $\Delta/2\pi = 2$ kHz and $\beta/2\pi = 1$ kHz. On-resonance CW decoupling with a field strength of $\omega_1^{\mathrm{H}}/2\pi = 160$ kHz was used during the sweep. After the adiabatic DREAM sweep, unwanted coherences were removed by a 90° pulse whose phase was par-

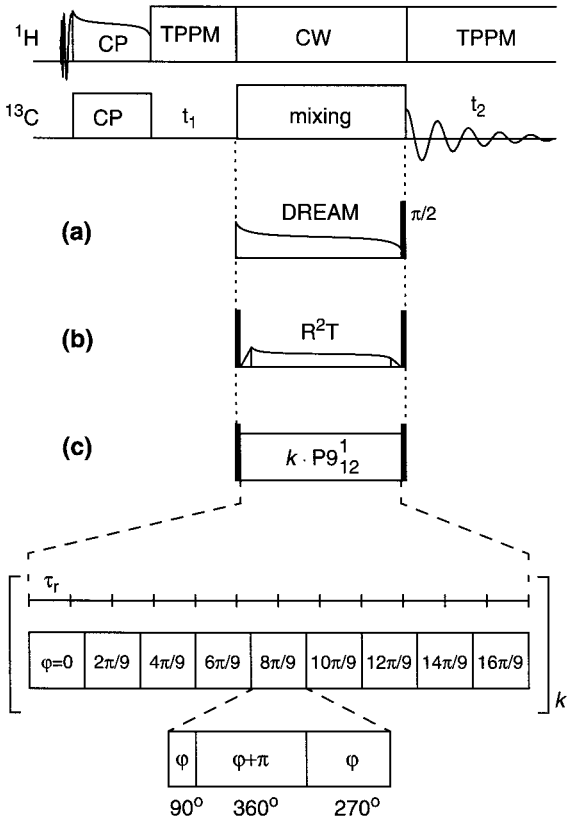

Figure 2. Pulse sequences for homonuclear correlation experiments. ^{13}C polarization is generated by adiabatic-passage Hartmann–Hahn cross polarization (APHH CP) with an adiabatic sweep replacing the initial 90° pulse. After an evolution time t_1, a recoupling sequence is applied during the mixing time τ under simultaneous application of high-power proton decoupling. (a) (Semi-)broadband dipolar transfer employing the DREAM sequence. (b) Frequency-selective dipolar transfer employing the R^2T sequence. (c) Broadband transfer via the J coupling employing the $P9^1_{12}$ TOBSY sequence. In the course of 12 rotor cycles, 9 rf cycles (POST elements (Hohwy et al., 1998)) are executed with their rf phase consecutively increased by $2\pi/9$ (Hardy et al., 2001). This supercycle is repeated k times.

allel to the sweep phase, but alternated in consecutive scans, while the receiver phase was kept constant.

The R^2T sequence is schematically shown in Figure 2b. After a short 'ramp-in' (RI) pulse, a tangential sweep was performed, followed by a short 'ramp-out' (RO) pulse. The time dependence of the applied rf-field strength during the tangential sweep again followed the general form of Equation 3, where ω_1^{HH} is to be replaced by the rf field at the rotational-resonance condition:

$$\omega_1^{RR} = \sqrt{\left(\frac{\omega_r}{2}\right)^2 - \left(\frac{\Delta\Omega^{iso}}{2}\right)^2} \qquad (5)$$

Here, $\Delta\Omega^{iso}$ is the average isotropic chemical-shift difference between the groups of resonances between which polarization transfer is desired. In our case $\Delta\Omega^{iso}$ was $2\pi \cdot 17.5$ kHz. The MAS frequency was chosen as $\omega_r/2\pi = 20$ kHz. The resulting rf-field strength at the rotational-resonance condition was $\omega_1^{RR}/2\pi = 4.8$ kHz. The length of the sweep was $\tau = 4.5$ ms, the shape parameters $\Delta/2\pi = 2.9$ kHz and $\beta/2\pi = 0.5$ kHz, with a 'down' shape (negative sign in Equation 3). The transmitter was centered approximately in the middle between the groups of resonances separated by $\Delta\Omega^{iso}$ at 92 ppm. For the RI and RO pulses, linear ramps with a duration of 20 μs were used.

^{13}C-^{13}C through-bond polarization transfer

For homonuclear transfer via the J coupling, the $P9^1_{12}$ TOBSY sequence (Hardy et al., 2001) was employed at a MAS frequency of $\omega_r/2\pi = 30$ kHz. At this MAS frequency, the required ^{13}C rf-irradiation strength is $\omega_1 = (3/2)\omega_r = 2\pi \cdot 45$ kHz. The pulse sequence for the $P9^1_{12}$ scheme is shown in Figure 2c. Efficient proton decoupling proved critical for the performance of the $P9^1_{12}$ sequence. We tried both on-resonance and Lee–Goldburg decoupling (Lee and Goldburg, 1965) with different decoupling field strengths during the mixing time. The best results were in both cases achieved with the highest fields that could be obtained with our probe, amounting to $\omega_1^H/2\pi = 160$ kHz, with similar efficiencies for on-resonance and Lee–Goldburg decoupling. To record correlation spectra, on-resonance decoupling with a 160 kHz decoupling field was chosen. It may be suspected that the performance of the sequence would increase further with still higher decoupling fields.

Experimental schemes

Two-dimensional homonuclear correlation experiments

Homonuclear correlation experiments were performed at a MAS frequency of 30 kHz with either the DREAM or the $P9^1_{12}$ TOBSY sequence for polarization transfer. An overview over the pulse sequences is shown in Figure 2.

For the experiments with DREAM mixing (Verel et al., 1998, 2001) (Figure 2a), the carrier frequency was set to the center of the aliphatic resonances at 39 ppm. This choice was due to the limited bandwidth of the DREAM sequence at 30 kHz MAS frequency

and 150 MHz ^{13}C resonance frequency, which does not allow to cover the full range of ^{13}C resonances. Phase-sensitive detection in the indirect dimension was accomplished using the TPPI scheme (Marion and Wüthrich, 1983). One thousand and twenty-four t_1 increments were recorded with a spectral width of 33 kHz; for each increment, four transients were co-added with an acquisition delay of 3 s, leading to a total acquisition time of ca. 3.5 h. For determining the transfer efficiency, an experiment with the DREAM mixing sequence and a control experiment without the sequence were performed, for each of which eight transients were co-added per increment.

For the TOBSY experiment (Hardy et al., 2001) (Figure 2c), the carrier was set to 94 ppm. The mixing time was 10.8 ms, corresponding to 27 $P9^1_{12}$ cycles. The number of t_1 increments and the spectral width were the same as for the DREAM experiment. For each increment, eight transients were co-added. A control experiment with the number of $P9^1_{12}$ cycles set to zero was performed.

Two-dimensional heteronuclear correlation experiments

Direct and relayed ^{15}N-^{13}C correlation experiments were recorded with the pulse sequences of Figure 3 at a MAS frequency of 20 kHz. For establishing direct correlations, the double APHH CP technique of Figure 3a was employed (Baldus et al., 1996). The carrier frequency on the ^{13}C channel was set approximately to the center of the spectrum at 84 ppm, and the shape parameters were tuned to yield similar polarizations in the C′ and C$^\alpha$ regions of the resulting spectrum. The TPPI scheme was used in the indirect dimensions. One hundred and seventy t_1 increments were recorded with a spectral width of 5 kHz. For each increment, 64 transients were co-added with a recycle delay of 5 s, leading to a total acquisition time of approximately 15 h.

To correlate the shift of each amide nitrogen N_k with the shift of the α carbon in the previous residue, C^α_{k-1}, selective ^{15}N-^{13}C cross polarization (Baldus et al., 1998) to the C′ nuclei followed by ^{13}C homonuclear polarization transfer by the R^{2}T sequence (Takegoshi et al., 1995, 1997; Costa et al., 1997) was employed (Figure 3b). This experiment is designated as an N(CO)CA experiment. During the ^{15}N-^{13}C cross-polarization step, the carrier of the ^{13}C channel was set to 185 ppm and the shape parameters were tuned to achieve selective cross polarization to the C′ spins. During the R^{2}T sequence and detection, the carrier was moved to the approximate center between the C′ and C$^\alpha$ regions at 92 ppm.

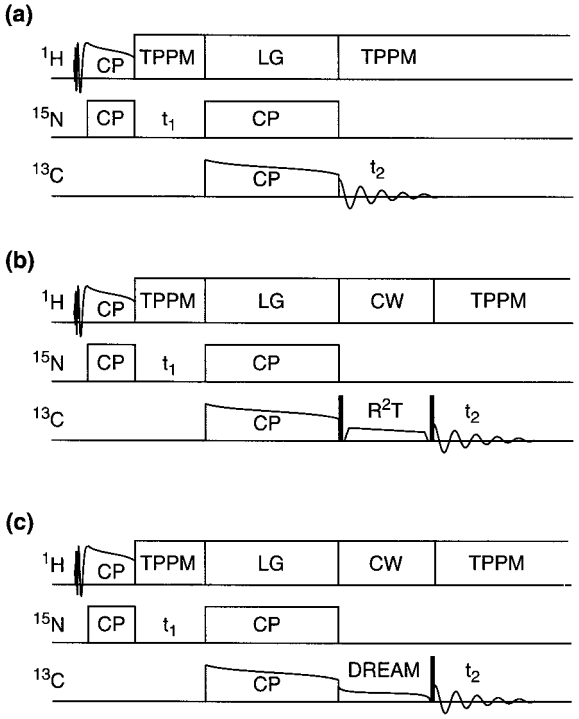

Figure 3. Pulse sequences for ^{15}N-^{13}C correlation experiments used in this work. (a) Direct ^{15}N-^{13}C shift correlation experiment via double APHH CP. (b) N(CO)CA experiment. The parameters of the second APHH step are chosen such that polarization is transferred preferentially from the ^{15}N spins to the ^{13}C′ spins. In the following R^{2}T step, this polarization is then transferred to the C$^\alpha$ spins. (c) N(CA)CB experiment. The parameters of the second APHH step are now tuned for preferential transfer to the C$^\alpha$ region. The resulting polarization is then transferred into the aliphatic side chains by a DREAM sweep.

To correlate the shift of each amide nitrogen N_k with the shift of the aliphatic side-chain carbons in the same residue, C^β_k, selective ^{15}N-^{13}C CP to the C$^\alpha$ nuclei was followed by ^{13}C homonuclear transfer by the DREAM sequence (Figure 3c). This experiment is called an N(CA)CB experiment. The carrier of the ^{13}C channel was set to 39 ppm for the whole experiment. The shape parameters for ^{15}N-^{13}C APHH CP were tuned to give maximum transfer to the C$^\alpha$ spins.

Three-dimensional correlation experiments

Three-dimensional (3D) ^{15}N-^{13}C-^{13}C chemical-shift correlation experiments (Sun et al., 1997) were performed by extending the sequence of Figure 3b by an additional ^{13}C evolution period immediately after the second APHH CP and before the R^{2}T mixing

sequence. The carrier of the ^{13}C channel was centered at 92 ppm during the whole experiment. The shape parameters of the ^{15}N-^{13}C APHH CP step were deliberately chosen such that similar amounts of polarization resulted on the C′ and C^{α} spins. In both indirect dimensions, phase-sensitive detection was accomplished with the TPPI scheme. In the indirectly detected ^{15}N dimension (t_1), 32 increments with a spectral width of 3 kHz were acquired; in the indirectly detected ^{13}C dimension (t_2), 256 increments with a spectral width of 35 kHz were recorded. For each increment, eight transients were co-added with a recycle delay of 5 s, leading to a total acquisition time of 91 h. An additional time-domain data set was created by extracting the data of the first eight t_2 increments from this data set, corresponding to a shortened 3D experiment with an acquisition time of 2 h 50 min.

Results and discussion

Influence of sample preparation

A careful preparation of the antamanide sample, ensuring a homogeneous, microcrystalline state, proved important for obtaining high-quality spectra. In order to illustrate the range of situations that may result from different sample-preparation techniques, some ^{13}C and ^{15}N spectra of differently prepared samples are shown in Figure 4. The lyophilized powder gives rise to broad resonances in the ^{13}C and ^{15}N spectra, the latter being almost featureless (Figure 4a). The situation improves significantly after recrystallization (Figures 4b and 4c) from a 7:3 methanol/water mixture. Similar improvements upon recrystallization have been observed in other biomolecules (Pauli et al., 2000). For the sample of Figure 4b, the solvent was evaporated within less than one day in the presence of dried silica gel as a drying agent. A 2D ^{13}C-^{13}C correlation spectrum of this sample (not shown) revealed a structural heterogeneity with at least two molecular conformations in the crystal or two different crystal forms. This heterogeneity is also reflected in line broadening and line splittings in the ^{15}N spectrum. A far more homogeneous, microcrystalline sample was obtained by slow recrystallization over a period of four days in a controlled humidity of 76%. One-dimensional spectra from this sample, which was used throughout the rest of this work, are shown in Figure 4c. Most of the ^{13}C and ^{15}N resonances are now well resolved. Typical linewidths for this sample are 60–100 Hz (0.4–0.7 ppm) for the ^{13}C resonances and 35–65 Hz (0.6–1.1 ppm) for the ^{15}N resonances.

Identification of the ^{13}C spin system of each amino acid

To establish the connectivities between the ^{13}C nuclei within each residue of antamanide, we employed 2D homonuclear through-space and through-bond correlation experiments. For the through-bond schemes, it is quite obvious that only correlations within one amino acid are established because the two-bond $^{13}C'$-N-$^{13}C^{\alpha}$ J couplings are smaller than the one-bond couplings by at least a factor of 30 (Kao and Barfield, 1985; Hu and Bax, 1997). For through-space transfer and short mixing times, only dipolar couplings between directly bonded ^{13}C nuclei yield cross peaks due to the r^{-3} distance dependence of the dipolar interaction, and a similar spectrum is obtained.

A through-space correlation spectrum obtained with the DREAM scheme is shown in Figure 5a. At the chosen combination of magnetic field (14 Tesla) and MAS frequency (30 kHz), the bandwidth of the DREAM sequence is not quite sufficient to achieve efficient recoupling over the entire chemical-shift range of the peptide. Therefore the transmitter frequency was centered at 39 ppm to achieve band-selective uniform recoupling in the region of the C^{α} and aliphatic side-chain resonances. At higher spinning frequencies ($\geq$40 kHz), however, a single DREAM experiment is broadband enough to cover the entire spectral range of ^{13}C at a static magnetic field of 14 T.

As expected for a double-quantum transfer mechanism, almost all cross peaks in Figure 5a exhibit negative intensity, shown in red color. Exceptions can be ascribed to two-step relayed transfer. Due to the sequential passage through the HORROR condition for different spin pairs, the spectrum is not symmetric around the diagonal (Verel et al., 2001). All cross peaks between aliphatic resonances are well resolved in the spectrum. Several factors may be responsible for the significantly higher resolution compared to the earlier study (Straus et al., 1997), including improved sample preparation and higher MAS spinning frequency in conjunction with TPPM decoupling and higher decoupling fields.

From the cross-peak pattern in Figure 5a, it is straightforward to assign the observed chemical shifts to specific amino acid types. A convenient starting point is given by the four intense cross peaks in the lower left corner of the spectrum, which are readily

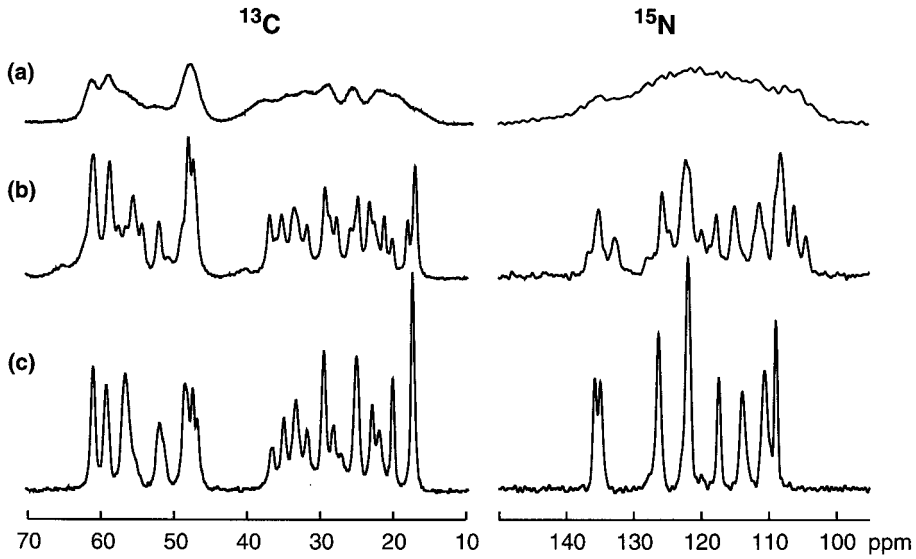

Figure 4. Selection of ^{13}C and ^{15}N MAS spectra of antamanide for different sample preparations. (a) Lyophilized powder. (b,c) Microcrystalline powder obtained by evaporation of the solvent from a solution of antamanide in a 7:3 methanol/water mixture. In the ^{13}C spectra, only the aliphatic region is shown. The sample leading to spectra (b) was obtained by fast evaporation of the solvent at room temperature in the presence of dry silica gel as a drying agent. The sample leading to spectra (c) was obtained by slow evaporation during several days in a controlled humidity of 76%. This sample was used throughout the rest of this work.

assigned to C^{α}-C^{δ} cross peaks of proline (marked P$\alpha\delta$) by the characteristic chemical shifts of the C^{δ} resonances. Having assigned the C^{α} and C^{δ} resonances, the cross peaks involving C^{β} and C^{γ} can easily be spotted. Identification of the single alanine is also straightforward by its intense C^{α}-C^{β} cross peak at the characteristic C^{β} frequency of 17.1 ppm. Having identified the alanine, the valine is easily recognized by the presence of the two-bond $C^{\gamma 1}$-$C^{\gamma 2}$ cross peak, and the cross peaks between the $\gamma 1$, β, and α resonances can now easily be pinpointed. The corresponding cross peaks that involve the $\gamma 2$ resonance are missing in the lower triangle but can only be found in the upper triangle or, alternatively, in the through-bond spectrum (vide infra). The remaining four cross peaks then belong to the four phenylalanines in antamanide. Most of the thus identified cross peaks are between directly bonded neighbors. Cross peaks which correspond to two-bond correlations are (with the exception of the valine $C^{\gamma 1}$–$C^{\gamma 2}$ and the proline C^{α}–C^{δ} cross peaks) much weaker or not visible at all for the chosen mixing time.

Having assigned all the intra-residue cross peaks, we could search for additional cross peaks indicating interresidue correlations. At the chosen mixing time of 7 ms, only a few very weak correlations between side-chain resonances of neighboring residues can be found; their intensity amounts to less than 1% of the total spectral intensity, and they are below the lowest contour level in Figure 5a. Stronger interresidue peaks can be generated by increasing the mixing time, i.e., by decreasing the rate of change of the DREAM Hamiltonian. For a mixing time of 14 ms, about 65 interresidue cross peaks can be identified in the spectrum (not shown). While most of these interresidue peaks are rather weak (typically about 2% of the maximum peak intensity in the spectrum), the intensity of some of these peaks exceeds 5% of the maximum peak intensity. Based on such interresidue peaks, in principle a full sequence-specific assignment of the carbon resonances can be achieved; this is the route followed in an earlier study (Straus et al., 1997). In this paper, however, we follow an alternative strategy for sequence-specific assignment, based on ^{15}N-^{13}C correlation spectroscopy (vide infra).

To identify the ^{13}C spin system of each amino acid it is also possible and indeed more intuitive to use polarization transfer through chemical bonds exploiting the J coupling. Figure 5b shows a TOBSY spectrum of antamanide obtained with the $P9^{1}_{12}$ mixing sequence for a mixing time of 10.8 ms. Linewidths in the DREAM (Figure 5a) and TOBSY spectra (Figure 5b) are comparable (vide infra); apparent differences are mostly due to different peak heights and different con-

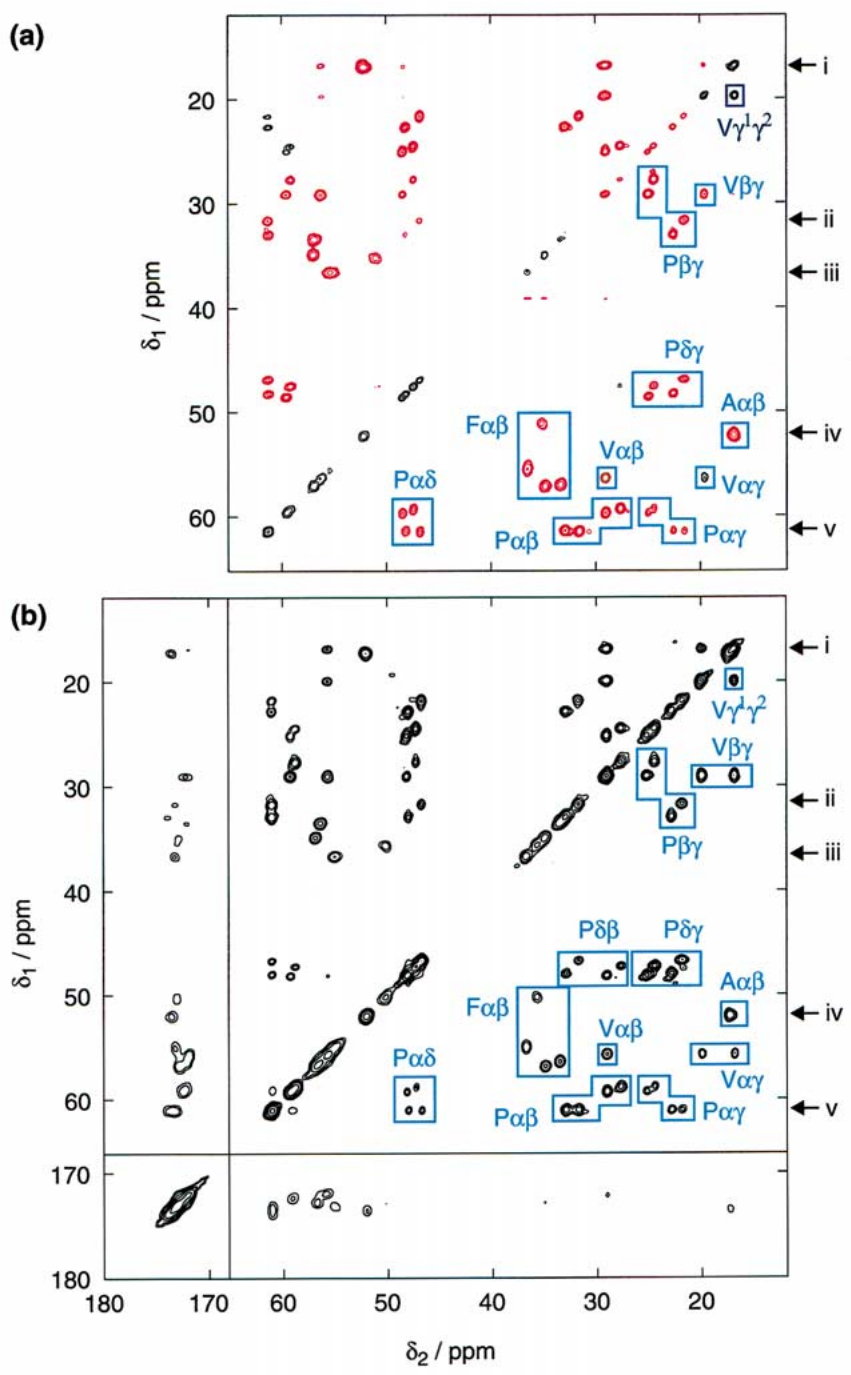

Figure 5. ^{13}C homonuclear shift-correlation spectra at a MAS frequency of $\omega_r/2\pi = 30$ kHz. (a) Spectrum obtained with the DREAM sequence for dipolar transfer with a mixing time of 7 ms. The total acquisition time was 3.5 h. Only the region containing the C^{α} and aliphatic side-chain resonances is shown. Negative intensity is indicated by red contours. Contours are at plus and minus 4%, 7%, 12%, 20%, 33%, and 57% of the maximum intensity. The spectrum readily allows to assign all cross peaks to their respective spin systems. These spin-system assignments are indicated for the cross peaks below the diagonal. (b) Spectrum obtained with the $P9^1_{12}$ TOBSY sequence for transfer via the J couplings. A mixing time of 10.8 ms, corresponding to 27 $P9^1_{12}$ supercycles, was chosen. The total acquisition time was 7 h. Contours are at 2.5%, 7%, 14%, 28%, and 54% of the maximum intensity. The spectrum yields most of the expected intra-residue correlations, including C'-C^{α} correlations. No artificial line narrowing, e.g., by applying a shifted window function to the time-domain data, was employed during processing for both spectra. To the right of each spectrum, the positions are indicated around which the 1D slices of Figure 6 were extracted.

tour levels. The bandwidth of the TOBSY sequence is sufficient to achieve polarization transfer over the complete chemical-shift range of the peptide, which is approximately 24 kHz. As in the DREAM spectrum, the strongest cross peaks are found between directly bonded neighbors in the aliphatic side-chain regions, for which the J coupling is in the range of 32 to 38 Hz (Bystrov, 1976). Cross peaks between the C' and C^{α} resonances are considerably weaker, despite the relatively strong coupling of typically 50 to 53 Hz (Bystrov, 1976) between such spins in peptides. This probably reflects imperfect suppression of both the large chemical-shift differences of up to 123 ppm (18.5 kHz) between these types of spins and of the large chemical-shift anisotropy of the carbonyl spins. The aromatic side-chain signals (not shown) were strongly attenuated by the TOBSY sequence due to the shorter $T_{1\rho}$ of these spins. Nevertheless, the cross peaks between the phenylalanine C^{γ} nuclei and the respective C^{β} were clearly visible and could be assigned, while the other phenyl resonances showed strong overlap.

Correlations are also visible between nuclei which are separated by more than one bond but still belong to the same spin system. Most of these cross peaks probably do not arise from direct transfer via the generally weak $^{2,3}J_{CC}$ couplings (Bystrov, 1976), but rather from relayed transfer between successive directly bonded neighbors. They are mostly stronger than in the DREAM spectrum. This can be rationalized by the fact that in the course of a DREAM sweep different spin pairs become recoupled sequentially (Verel et al., 2001), while in the TOBSY experiment all spins are coupled simultaneously during the entire mixing period. Apart from the attenuation of the aromatic resonances and the overall linewidths, the TOBSY spectrum is in fact very similar to a ^{13}C TOCSY spectrum (Braunschweiler and Ernst, 1983; Fesik et al., 1990) at the same field strength obtained from a sample of antamanide dissolved in chloroform (spectrum not shown). In particular, the solution-state spectrum also features the relatively strong $P\alpha\delta$ cross peaks.

For a quantitative evaluation of the efficiencies achieved by the two transfer schemes, we recorded spectra with identical parameters as in the spectra of Figure 5, but once with and once without a mixing sequence applied. Some selected 1D sum projection slices of these spectra are shown in Figure 6a for the DREAM sequence and in Figure 6b for the TOBSY sequence. The slices were generated by integrating strips of 0.8 ppm width along δ_1 centered at the positions indicated at the right side of Figure 5. Based on the assignments reported below, these chemical-shift values correspond to the nuclei indicated in the center of Figure 6. It is these nuclei on which the polarization is localized at the start of the t_1 period of the correlation experiments. The initial polarization is directly detected in the control experiments (dotted traces in Figure 6) to allow for a quantification of the transfer efficiency and the relaxation losses. At the same time, the traces allow us to get a direct impression of the linewidths in the correlation spectra.

For the further discussion, we define a normalized transfer efficiency η_N in a specific spectral region by the ratio of the absolute cross-peak intensity to the sum of the absolute intensities of diagonal and cross peaks. This figure indicates how much of the polarization actually detected in a correlation experiment is found in the cross peaks. The higher η_N, the higher the cross peak intensity relative to the diagonal in a correlation experiment. We further define an absolute transfer efficiency η as the ratio of the absolute cross-peak intensity in the correlation spectrum to the total intensity (localized in the diagonal region) in the control spectrum. This figure indicates how much of the initial polarization is finally detected in the spectral regions of interest. It is this figure that is relevant for sensitivity considerations; it includes all losses experienced by the spin system during the transfer. Clearly, always $\eta \leq \eta_N$.

From the traces of Figure 6a, it is obvious that the DREAM transfer scheme achieves high normalized efficiencies η_N, as most of the intensity of the displayed slices is found in the cross peaks. Indeed, for the solid trace (ii), no diagonal peak intensity was detected at all down to noise level, and thus for this slice, $\eta_N = 100\%$. On average, for the whole spectral region shown in Figure 5a, $\eta_N = 85\%$. Furthermore it is obvious that, certainly for some slices, the absolute efficiency η is considerably lower than η_N. Take, e.g., again trace (ii) of Figure 6a. Only a fraction of 33% of the initial polarization (dotted trace) actually survives in the correlation experiment (solid trace) for this slice, even though all the polarization is found in the cross peaks ($\eta = 33\%$, but $\eta_N = 100\%$). On the other hand, for trace (v), 57% of the initial polarization appears as cross-peak intensity, which means $\eta = 57\%$. Overall, for the spectrum of Figure 5a, η varies between 29% and 57%, with an average value of 42%. Comparing the latter number to the average $\eta_N = 85\%$, we can quantify the total magnetization loss due to

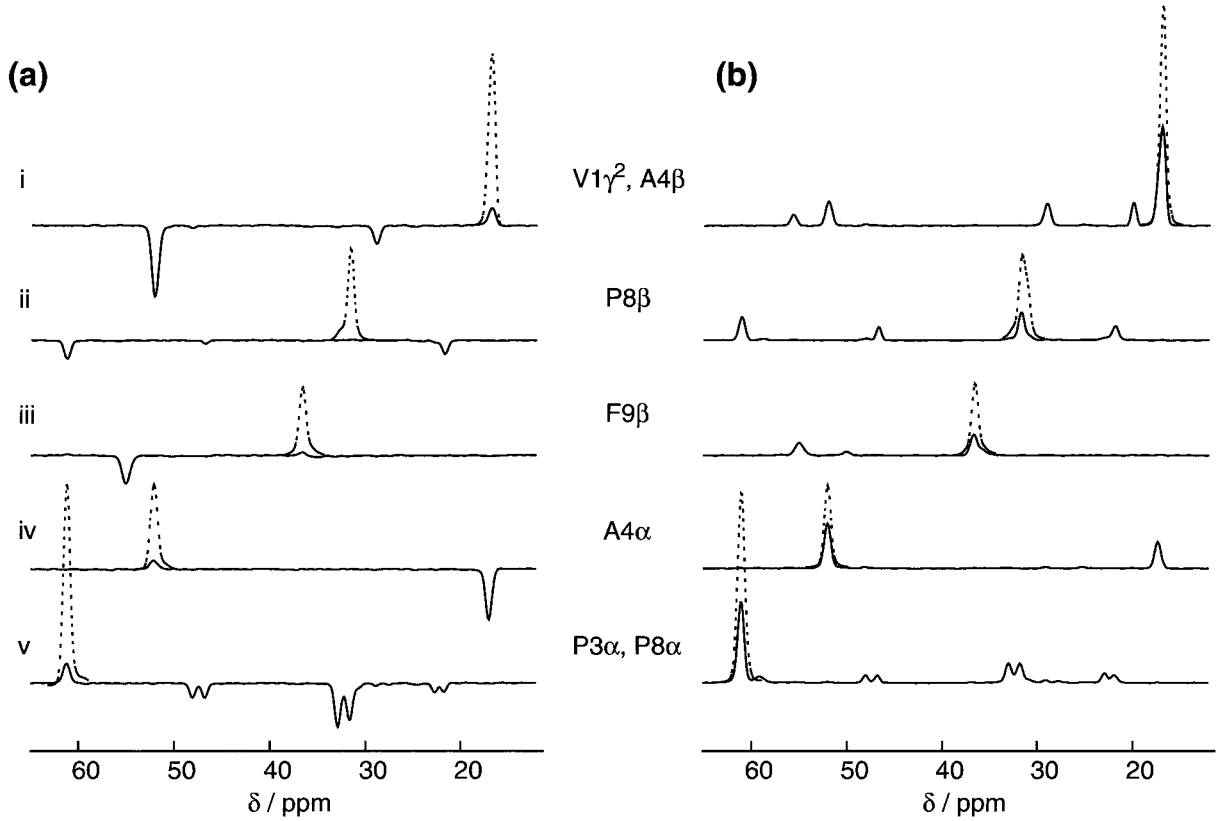

Figure 6. Partial 1D projection slices of 2D spectra without (dotted traces) and with (solid traces) a mixing sequence applied. (a) DREAM, (b) $P9^1_{12}$ TOBSY. The acquisition time for each 2D spectrum was 7 h. Slices were generated by integrating the corresponding 2D spectrum along δ_1 over a strip of 0.8 ppm width centered at the following chemical shifts: (i) 17.0 ppm, (ii) 31.5 ppm, (iii) 36.5 ppm, (iv) 52.1 ppm, (v) 61.1 ppm. These shifts correspond to the ^{13}C nuclei given in the center row of the figure. Each slice thus shows how initial polarization (dotted trace) on the given ^{13}C nuclei is distributed onto other nuclei by the mixing sequence (solid trace).

experimental imperfections and dissipative processes to about 50%. We tentatively attribute a significant part of the losses to imperfect proton decoupling.

For the TOBSY experiment, the traces of Figure 6b show that a substantial amount of polarization remains on the diagonal. Thus η_N is somewhat lower than for the DREAM experiment, with an average of $\eta_N = 49\%$. With the exception of trace (ii), also the absolute efficiency in the displayed slices is lower than for the DREAM experiment. For the aliphatic region, η varies between 20% and 59%, with an average of 32%. Much lower efficiencies are found for polarization initially localized on carbonyl or aromatic carbons, as can be seen by the low intensity of the cross peaks in the lower region of Figure 5b. The reasons for the lower performance of the TOBSY experiment as compared to the DREAM experiment are probably twofold. On the one hand, there is a distribution of J-coupling constants among the different spin pairs involved in the transfer. Therefore, for a given mixing time τ, the transfer can only be at its maximum for those spin pairs which have a J coupling of approximately $1/2\tau$. On the other hand, the mixing time in the TOBSY experiment was 50% longer than the DREAM sweep, and the TOBSY pulse sequence has no effective spin-lock field. Both effects can lead to increased loss of spin order.

Nevertheless, the information content of the TOBSY spectrum in Figure 5b is somewhat higher than that of the DREAM spectrum in Figure 5a, owing to the increased bandwidth of the TOBSY sequence. Furthermore, the TOBSY spectrum is fairly symmetric about the diagonal, and there are no missing cross peaks on either side. The C′ and the phenylalanine C^γ resonances can easily be assigned to their respective spin systems with the help of this spectrum. Therefore, the TOBSY experiment seems to be a superior alternative to dipolar coupling-based polarization-transfer

schemes. In systems with large-amplitude motions, however, the longer mixing time of a TOBSY experiment may make it less favorable than dipolar coupling-based polarization transfer using DREAM, for which the mixing time could be reduced by an additional factor of two with only modest losses in transfer efficiency.

Sequential assignment of the backbone resonances

Direct ^{15}N-^{13}C correlations

For the sequential assignment we performed triple-resonance experiments that establish a correlation between the spin systems belonging to amino acids that are neighbors in the primary sequence. A direct ^{15}N-^{13}C chemical-shift correlation spectrum obtained with the APHH CP pulse sequence of Figure 3a is shown in Figure 7a. Inspection of the spectrum shows that for the applied contact time of $\tau_{CP} = 8$ ms, only directly bonded ^{13}C neighbors were cross polarized from each ^{15}N spin. The spectrum, therefore, correlates each amide nitrogen N_k with the carbonyl carbon C'_{k-1} of the preceding residue, with C^{α}_k of the same residue, and, for the proline residues, with C^{δ}_k. The proline residues can be identified immediately by the presence of these C^{δ} cross peaks. For antamanide, the full sequential backbone assignment can already be completed at this point: using the C^{α} and C' assignments obtained from the homonuclear correlation experiments, the ^{15}N-^{13}C spectrum establishes the missing link between the C'_{k-1} and C^{α}_k resonances of neighboring residues by connecting them via the common amide nitrogen N_k. However, because of the considerably larger frequency spread in the C^{α} region than in the (more crowded) C' region, we will instead proceed with an assignment strategy in which sequential assignment is based primarily on C^{α} resonances.

In the direct correlation experiment, the APHH pulse parameters (vide supra) were adjusted such that similar intensities were reached in the C' and $C^{\alpha,\delta}$ regions of the spectrum. It may be illustrative to compare the obtained signal intensities of these regions to the corresponding intensities after direct ^{1}H-^{13}C CP. The sum intensity of the C' and $C^{\alpha,\delta}$ regions in the double APHH CP experiment amounts to 21% of the sum intensity of these regions after direct APHH CP from the protons to carbons with 1 ms contact time. Experimentally, this figure does not change significantly when the rf-irradiation frequency, rf-field strength at the Hartmann–Hahn condition, and direction of the amplitude sweep (up or down) are varied within reasonable limits. What does change, however, is the relative ratio of intensities of the C' and $C^{\alpha,\delta}$ regions, including the possibility of achieving rather selective transfer to one of the regions only and thereby achieving a higher sensitivity in a specific region. In order to quantify the combined efficiency of the ^{1}H-^{15}N and ^{15}N-^{13}C transfer steps, we first consider a situation in which polarization is transferred from one ^{15}N spin to only one ^{13}C spin. If the ^{15}N-^{13}C transfer is perfectly adiabatic, all ^{15}N polarization is transferred to the ^{13}C spin, and the same final intensity results on the ^{13}C spin as after a direct ^{1}H-^{13}C CP, assuming the same performance of the CP from the protons to either ^{13}C or ^{15}N. In the nonselective experiment discussed here, however, the polarization which after ^{1}H-^{15}N CP is localized on one ^{15}N spin per residue gets spread out onto two ^{13}C spins (three for prolines) in the second CP step. Using an oversimplified thermodynamic model, neglecting the details of the spin dynamics (Sørensen, 1990), we expect that the sum polarization on the two (three) ^{13}C spins after ^{15}N-^{13}C CP is roughly the same as if the polarization of each ^{15}N spin was transferred to one ^{13}C spin only. To estimate the efficiency of the double ^{1}H-^{15}N-^{13}C CP versus direct ^{1}H-^{13}C CP, we therefore have to scale the total intensity of the C' and $C^{\alpha,\delta}$ regions after the direct ^{1}H-^{13}C CP experiment with the ratio of the numbers of ^{15}N versus ^{13}C spins involved in the double CP. For antamanide, this number is 10/24, leading to a theoretical sum intensity of 42% for the double CP relative to direct CP in the spectral regions considered here. The experimental intensity of 21% indicates that an efficiency of about 50% was realized for the double CP relative to direct CP.

Relayed ^{15}N-^{13}C correlations via homonuclear ^{13}C-^{13}C transfer

By the direct correlation experiment, we have already established a correlation between each amide nitrogen N_k and the α carbon C^{α}_k in the *same* residue. We now aim at obtaining a correlation of N_k with C^{α}_{k-1} in the *previous* residue. To achieve this correlation, we employed selective ^{15}N-^{13}C cross polarization to the C' nuclei followed by homonuclear ^{13}C polarization transfer. Several homonuclear ^{13}C mixing schemes including TOBSY sequences could be envisaged for this step. In choosing the most suitable sequence, we were led by sensitivity considerations: as discussed above, much sensitivity is lost by spreading out polarization that was initially localized on a small number of spins onto a larger group of spins. We therefore aim at

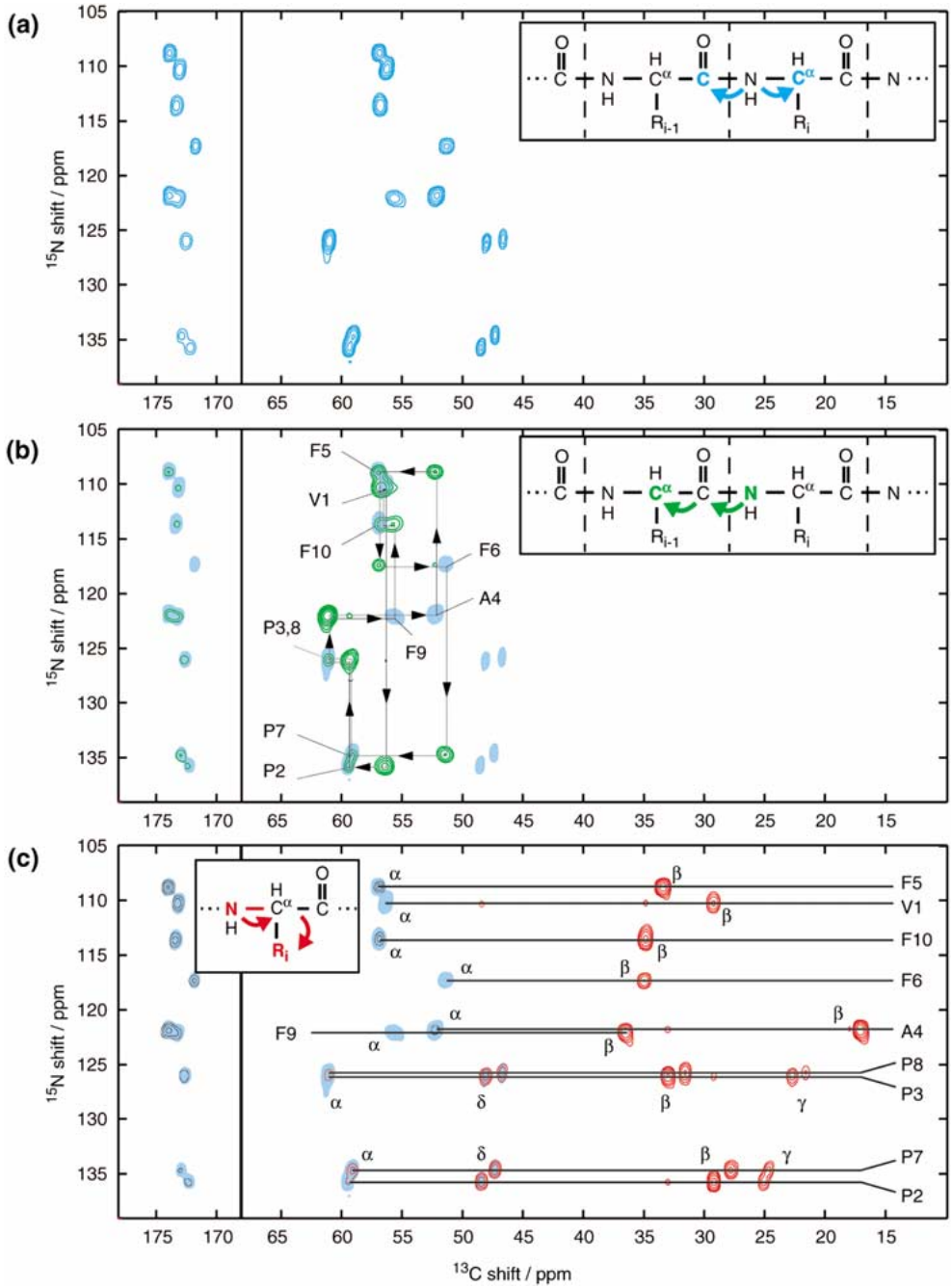

Figure 7. ^{15}N-^{13}C correlation spectra of antamanide. (a) Direct N-C correlation obtained with the pulse sequence of Figure 3a. Each amide nitrogen N_k is correlated with the directly attached carbons C^{α}_{k} in the same residue and C'_{k-1} in the previous residue. Contours are at 7%, 12%, 20%, 35% and 59% of the maximum intensity. (b) N(CO)CA correlation obtained with the sequence of Figure 3b. This spectrum, shown in green contours, correlates each amide nitrogen N_k with the α carbon of the previous residue, C^{α}_{k-1}. Contours are at 10%, 15%, 22%, 32%, 46%, and 68% of the maximum intensity. The peak positions of the spectrum of part (a) are indicated by light blue areas. By 'walking' through these two spectra in a stepwise fashion as indicated by the arrows, all ^{15}N and ^{13}C resonances can be assigned in a sequence-specific way. (c) N(CA)CB correlation obtained with the sequence of Figure 3c. In this spectrum, each amide nitrogen N_k is correlated with the aliphatic side-chain carbons in the same residue k. Positive intensity is indicated by black, negative by red contours, with contour levels at plus and minus 7%, 12%, 20%, 35% and 59% of the maximum absolute intensity. The peak positions of the spectrum of part (a) are again indicated by light blue areas.

keeping polarization localized on as few spins as possible ('minimum spread'). Being led by this criterion, we selected a sequence that selectively and efficiently transfers polarization from the C′ nuclei to the neighboring C^{α} nuclei. This can be achieved by an adiabatic passage through the rotational-resonance condition in the presence of rf irradiation, also called the rotational-resonance tickling (R^2T) experiment (Takegoshi et al., 1995, 1997; Costa et al., 1997). R^2T is selective for a narrow band of chemical-shift differences somewhat smaller than but close to the MAS frequency. By selecting the shape of the rf amplitude, the width of the recoupling condition was adapted to the particular needs.

In the R^2T experiment, the MAS frequency is determined by the frequency difference of the recoupled spins: in antamanide, the difference between the centers of the isotropic chemical-shift distributions of the C^{α} and C′ spins amounts to 116 ppm or 17.5 kHz, ranging from 16.9 to 18.4 kHz. We have, therefore, chosen a MAS frequency of 20 kHz for all heteronuclear correlation experiments. The R^2T experiment is, however, the only one out of the set employed here that requires a certain, relatively well-defined MAS frequency. For the magnetic field used, the choice of 20 kHz at the same time avoids any unwanted rotational-resonance recoupling condition between the C′ spins and other carbons, placing the C′ spinning sidebands into the empty spectral region between the C^{α} and aliphatic side-chain regions.

The resulting spectrum, obtained with the N(CO)CA sequence of Figure 3b, is shown in Figure 7b with green contours. For each N_k chemical-shift position, we find a strong peak associated with the C^{α}_{k-1} resonance of the previous residue. These peaks are not present in the direct correlation spectrum shown in Figure 7a (the peak positions of Figure 7a are indicated by blue areas in Figures 7b and c). Peaks that correspond to C^{α} and C′ resonances attached directly to the respective nitrogen are also present, but strongly attenuated, indicating a good selectivity of the ^{15}N-^{13}C APHH CP and a high adiabaticity of the R^2T transfer. We determined the absolute transfer efficiency of the R^2T step in antamanide by a homonuclear correlation experiment with the pulse sequence of Figure 2b. The efficiency η varied in the range from 40% to 66% for the different residues, with an average of 57%. The transfer from C′ to C^{α} is close to being complete, expressed in an average normalized transfer efficiency of $\eta_N = 82\%$ for the R^2T step. These numbers might have to be somewhat modified if the efficiencies in the triple-resonance experiment are to be considered: the ^{15}N-^{13}C APHH CP step preceding the R^2T step may excite preferentially certain parts of the sample volume due to the inhomogeneity of the B_1 fields, for which in turn R^2T might perform better or worse than average over the complete sample volume.

Sequential assignment of the C^{α} resonances is now straightforward: We start from an arbitrary N_k-C^{α}_k cross peak in the direct correlation spectrum. We now look for an N-C^{α} peak at the same ^{13}C frequency in the N(CO)CA spectrum (vertical lines in Figure 7b). This peak is the N_{k+1}-C^{α}_k cross peak. Going back to the direct correlation spectrum, we look for the N_{k+1}-C^{α}_{k+1} cross peak at the same ^{15}N frequency (horizontal lines). By this procedure, a full sequential ^{15}N, $^{13}C^{\alpha}$ assignment is achieved. Note that there are some potential ambiguities in this procedure, as some of the peaks in Figure 7b overlap. This leads to several possibilities to connect these peaks. These ambiguities can, however, be resolved by taking the results from the homonuclear correlation experiments into account. This can easily be verified by starting with the resonance marked A4, which can be uniquely assigned to the C^{α} resonance of Ala4, and continuing along the arrows. All possibilities of departing from the connections drawn can immediately be ruled out by the known primary sequence of the peptide and the known assignments of the resonances to amino acid types.

After a complete assignment of the C^{α} resonances has been achieved, the carbonyl and side-chain resonances can now be assigned in a sequence-specific manner by going back to the homonuclear correlation spectrum discussed above and using the sequential assignments of the C^{α} resonances to label the identified spin systems sequentially. The resulting resonance assignments are given in Table 1.

In the present study, the combination of two heteronuclear 2D correlation experiments and one homonuclear 2D correlation experiment, namely a direct and a relayed ^{15}N-^{13}C experiment and either a DREAM or a TOBSY experiment, was sufficient to achieve a full sequential assignment of all backbone and side-chain resonances. In larger polypeptides, peak overlap may render the assignment non-unique. In such cases, an additional experiment might be useful in which polarization is selectively transferred from the amide nitrogens to the aliphatic side-chain carbons through the C^{α} carbons. We performed such an N(CA)CB experiment on antamanide using the pulse sequence of Figure 3c. The N-C transfer was now tuned to give maximum transfer to the C^{α} region.

Table 1. Isotropic chemical shifts in (U-^{15}N,^{13}C) antamanide in ppm[a]

Residue	N	C′	Cα	Cβ	Cγ	Cδ,ε,ζ
Val1	110.4	172.3	56.3	29.2	19.8/17.0	–
Pro2	136.0	172.7	59.4	29.1	25.1	48.4
Pro3	126.2	174.0	61.0	33.0	22.7	48.0
Ala4	122.0	174.0	52.1	17.1	–	–
Phe5	108.9	171.9	56.9	33.4	139.0	[b]
Phe6	117.5	173.0	51.2	35.0	138.0	[b]
Pro7	134.9	172.9	59.0	27.8	24.6	47.3
Pro8	126.1	173.4	61.1	31.5	21.7	46.7
Phe9	122.2	173.5	55.5	36.5	138.3	[b]
Phe10	113.7	173.2	56.8	34.9	138.0	[b]

[a]The estimated uncertainty of the shifts is better than ±0.3 ppm for all resonances.
[b]These values could not be determined uniquely because of line broadening and overlap.

For the homonuclear transfer step, we employed the DREAM scheme with 20 kHz spinning. DREAM at such a relatively low MAS frequency is band selective. It is broadband enough to cover the aliphatic chemical-shift range, here specifically C^{α}-C^{β} pairs, while the unwanted transfer from C^{α} to C′ is quite inefficient. The resulting spectrum is depicted in Figure 7c. Under ideal conditions, the experiment would yield just N_k-$C_k^{\beta,\gamma,\delta,\cdots}$ cross peaks, with most of the intensity concentrated on the C_k^{β} spins. From the spectrum it is immediately apparent that the practical performance is quite satisfactory: C′ and C^{α} and resonances are much weaker than C^{β}. The DREAM step achieves almost perfect polarization transfer in this experiment, with $\eta_N = 90\%$ for the region between 15 and 65 ppm. The signal patterns in Figure 7c clearly confirm the assignments in Table 1. Similar experiments have recently been reported for a 62-residue protein (Pauli et al., 2001).

It is interesting to compare the assignments and chemical shifts found in this study to those in a similarly prepared solid phase (Straus et al., 1997) and in solution in chloroform (Kessler et al., 1989b) and dioxane (Ernst, 1993). An important difference to the earlier work in the solid state is immediately apparent: Whereas in the earlier solid-state NMR study (Straus et al., 1997) *two* distinct valine rotamers were identified, only *one* rotamer was found in the present investigation. We cannot rule out the existence of a second rotamer in our sample, but can give an upper limit of 2% for its relative occurrence from considering the signal-to-noise ratio of our homonuclear correlation experiments. Our sample is therefore well characterized by a single conformation for the valine side chains.

The differences between the carbon chemical shifts determined in the present study and those by Straus et al. (1997), Kessler et al. (1989b), and Ernst (1993), respectively, are plotted in Figure 8. The already noted conformational differences between the solid sample used here and that in the earlier solid-state work (Straus et al., 1997) are reflected in some relatively large chemical-shift differences, e.g. for the Val1 C^{α} resonance, which amount to 2.8 ppm and 1.7 ppm, respectively, for the two rotamers identified in the earlier work. The effect of the sample preparation on the ^{15}N shifts is at least as pronounced or even larger, as demonstrated in Figure 4. Relatively large shift differences are also found for the C′ resonances of Ala4 and Phe10 and for the β carbons of Phe5 and Phe6. All other observed shifts agree to within 1.5 ppm, mostly to within 1.0 ppm. A remarkable agreement is found between the shifts of the backbone and aliphatic side-chain resonances in the present study and in chloroform solution (Kessler et al., 1989b). All differences are smaller than 1.7 ppm, with the exception of the α carbon of Ala4 and the γ carbon of Phe6. The similarity in the observed shifts reflects the known similarity of the (average) molecular structure in chloroform solution with the molecular structure in the solid state (Kessler et al., 1989a). However, larger differences between the solid and solution shifts in chloroform are observed for the carbonyl carbons. This is not unexpected and reflects the different hydrogen bonding in the (water-rich) solid as compared to a solution in an essentially water-free, apolar solvent. On the other hand, significant differences of up to 4.6 ppm exist between the shifts of side-chain carbons in the solid and those in dioxane (Ernst, 1993), a polar solvent. These differences emphasize the importance of performing an independent resonance assignment of the solid material if solid-state NMR work is to be performed on peptides with known solution shifts.

Extension to 3D spectroscopy

Even though reasonably high transfer efficiencies and a high degree of selectivity in the transfer steps have been achieved in the 2D ^{15}N-^{13}C correlation experiments, the performance of these experiments is not ideal. As an example, let us reconsider the relayed N(CO)CA experiment of Figure 7b. Ideally, only N_k-C_{k-1}^{α} cross peaks should be present in this spectrum.

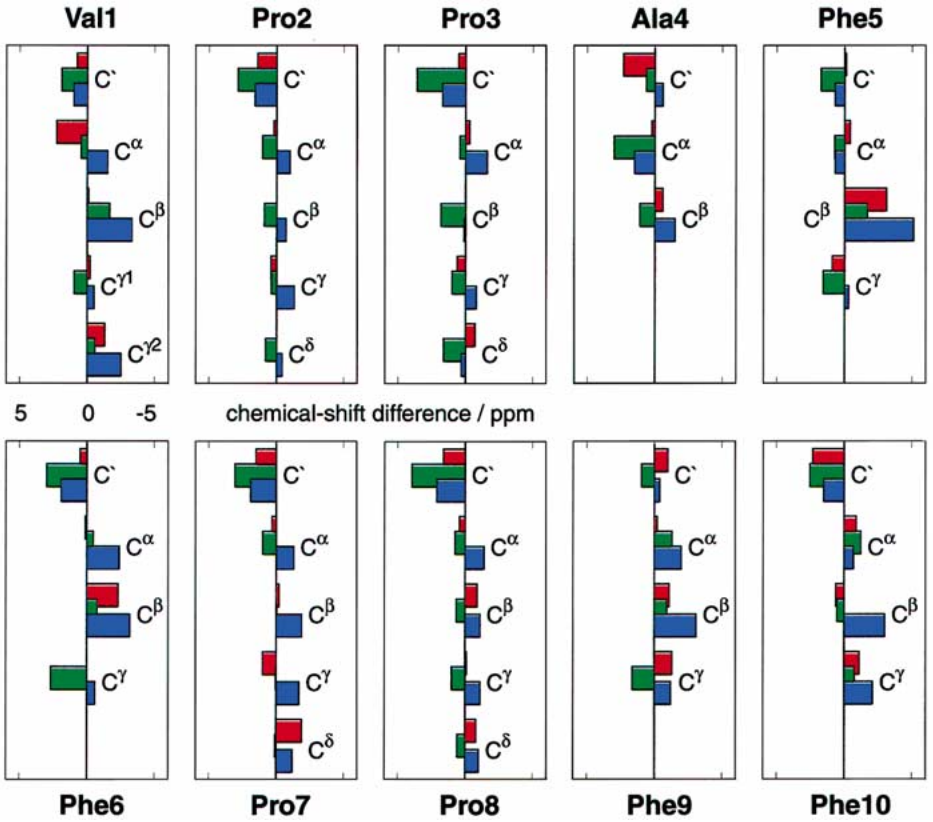

Figure 8. Deviations between the ^{13}C chemical shifts of antamanide determined in the present work and those determined earlier in the solid (red (Straus et al., 1997)), in chloroform solution (green (Kessler et al., 1989b)), and in dioxane solution (blue (Ernst, 1993)).

However, due to imperfect selectivity of the N-C transfer and imperfect adiabaticity of the R^2T transfer, some direct N_k-C_k^α peaks are also observed. In the present study these peaks do not significantly complicate the analysis, as they can be identified easily by comparison with the direct correlation spectrum of Figure 7a. In more complicated systems, however, identification of such unwanted peaks might not be as easy and unambiguous. A higher degree of selectivity of the N-C transfer step would resolve this problem, but might not be attainable.

In such cases, it is useful to extend the discussed techniques to three dimensions, thereby separating the correlations of the ^{15}N spins with the directly attached ^{13}C spins from those with further ('relayed') ^{13}C spins. Three-dimensional ^{15}N-^{13}C-^{13}C shift correlation experiments under MAS have been proposed in connection with non-adiabatic techniques for polarization transfer (Tycko, 1996; Sun et al., 1997; Rienstra et al., 2000) and were recently applied to the partial resonance assignment in the 76-residue protein ubiquitin (Hong, 1999). It is obvious that the application of *adiabatic* methods for transferring polarization can be advantageous also in the context of 3D spectroscopy. We performed 3D experiments by extending the N(CO)CA pulse sequence of Figure 3b by an additional evolution period after the ^{15}N-^{13}C CP step. The ^{15}N-^{13}C APHH CP step was deliberately chosen to be non-selective for either C′ or C^α in order to demonstrate the possibility of separating the direct and relayed correlations from both sides of the linking amide nitrogen by 3D spectroscopy.

The additional resolution gained by introduction of a third dimension is demonstrated in Figure 9, which shows a series of 2D slices at constant ^{15}N frequency from a 3D NCOCA spectrum. For each amide nitrogen N_k, the following peaks are expected: C_k^α and C'_{k-1} diagonal peaks (direct N-C correlations), and C'_{k-1}-C^α_{k-1} and C_k^α-C'_k cross peaks (relayed N-C correlations). Indeed, each of the displayed slices contains just these four well-separated peaks due to the good resolution along the ^{15}N dimension. Peaks at the same

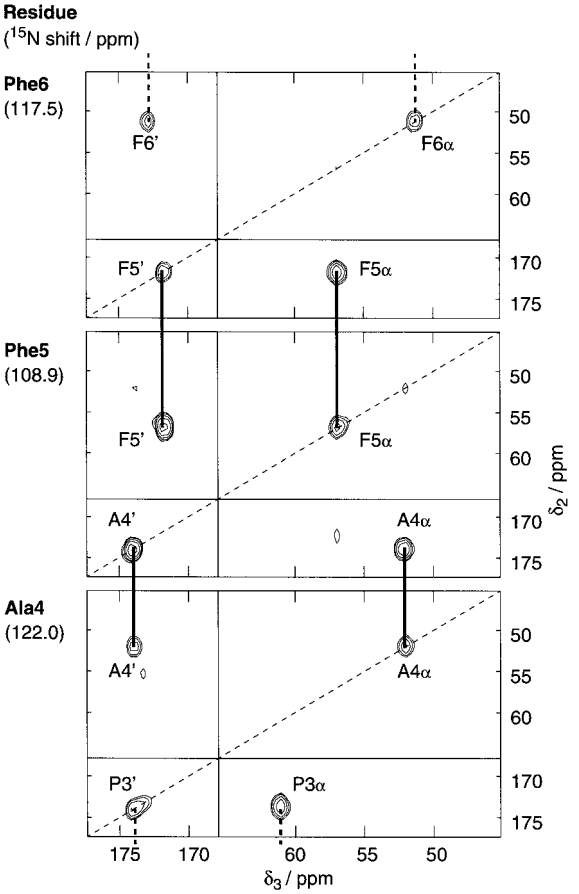

Figure 9. Slices of a 3D ^{15}N-^{13}C-^{13}C correlation spectrum of antamanide for constant ^{15}N chemical shift. After three-dimensional Fourier transformation, slices were extracted at the ^{15}N chemical shifts of Ala4, Phe5, and Phe6, respectively. Contours are at 19%, 26%, 38%, and 60% of the maximum intensity of each slice. Each slice contains diagonal peaks of the carbons directly attached to the corresponding ^{15}N nucleus, and cross peaks from these carbons to the next carbons along the backbone. In subsequent residues, identical frequency patterns appear along the directly detected carbon dimension (δ_3) at different positions in the indirectly detected carbon dimension (δ_2). Thereby a sequence-specific assignment can be completed, as indicated by the bold vertical lines.

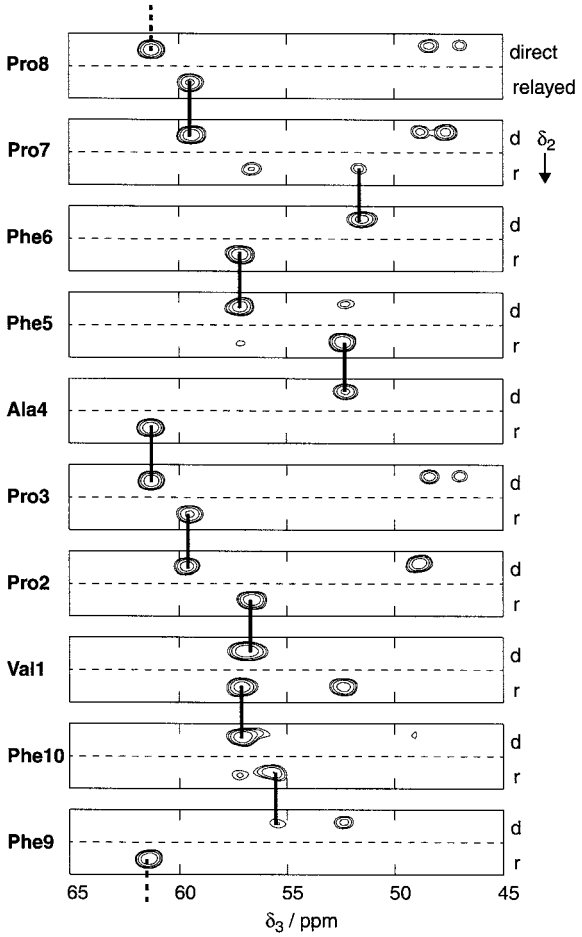

Figure 10. Slices of a 3D ^{15}N-^{13}C-^{13}C correlation spectrum with reduced resolution along the indirectly detected carbon dimension δ_2. Only eight t_2 increments were recorded. Slices were extracted at the amide nitrogen chemical shift of each residue. Contours are at 25%, 31%, 43%, and 64% of the maximum intensity. In the displayed region, each slice contains diagonal peaks from the α carbons directly connected to the ^{15}N nuclei resonant at the frequency of each slice, and cross peaks from α carbons connected indirectly to the same ^{15}N nuclei via an intermediate ^{13}C′ nucleus (relayed correlation). The resolution along δ_2 is just sufficient for distinguishing direct from relayed correlations. The connections of direct and relayed C$^{\alpha}$ signals between different slices, which lead to sequence-specific assignment, are again indicated by bold vertical lines.

δ_3 frequencies are found again in the corresponding slices of the next or previous residues, respectively. Thus, by connecting the slices as indicated by the bold vertical lines, an independent sequence-specific assignment can be completed. Thereby we could once more confirm our assignments obtained from combining information from 2D spectra.

The key information gained from the additional dimension δ_2 here is the separation of direct and indirect N-C correlations along this dimension. While for the spectrum of Figure 9 a relatively large number of t_2 increments were recorded (256), leading to a total acquisition time of 91 h, actually only very few increments (with a correspondingly shorter acquisition time) are needed to achieve this goal. This is demonstrated in Figure 10, where only eight t_2 increments (acquisition time 3 h) were used in conjunction with a cos^2 apodization filter in the t_2 dimension. Slices at constant amide ^{15}N shift are shown in Figure 10 for all

residues. Only the C^{α} region is displayed along δ_3. For each amide nitrogen N_k, a C^{α}_k diagonal peak (direct N-C correlation) and a C'_{k-1}-C^{α}_{k-1} cross peak (relayed N-C correlation) are expected. Indeed, for several slices just these two peaks appear. For other slices, the number of peaks is doubled because of spectral overlap of ^{15}N signals from two different residues, and for proline residues, also the C^{δ} resonances appear. Peaks from carbons directly attached to the amide nitrogen appear at different positions along δ_2 than peaks from remote carbons arising from relayed correlations. Despite the large linewidth along this dimension, the two types of peaks are perfectly separated, allowing for the same type of analysis as described for Figure 9.

The possibility of recording a meaningful 3D experiment with so few increments in t_2 relies on the almost perfect selectivity of the involved adiabatic R^2T homonuclear polarization transfer, which ensures that only C'-C^{α} cross peaks are found in each ^{13}C-^{13}C slice. 3D experiments of this type are an attractive alternative to 2D N(CO)CA experiments, as they can yield more information than a 2D experiment acquired in a comparable time, with a similar signal-to-noise ratio.

Conclusions

The sequential assignment of the ^{15}N and ^{13}C resonances in antamanide was demonstrated on a sample of 10 mg (about 8 μmol) of uniformly labelled material. The experimental schemes were, where possible, based on adiabatic pulse schemes. The efficiency of the transfer steps was characterized, and absolute transfer efficiencies up to 59% were found.

The resonances belonging to a single amino acid were identified by dipolar or J correlations. A single spectrum obtained by a broadband correlation experiment was sufficient for the spin-system assignment. Both methods proved to be applicable to our problem with a slight advantage for the TOBSY method. The employed TOBSY sequence $P9^1_{12}$ proved to be robust and achieved a reasonable absolute efficiency which, on average, amounted to 32% for aliphatic carbons. With an rf field requirement of $\omega_1 = (3/2)\omega_r$ on the carbon channel, the sequence puts only moderate demands on the NMR probe at MAS frequencies around 30 kHz. At a magnetic field of 14.09 T (600 MHz), the applied $P9^1_{12}$ sequence was broadband enough to cover the full chemical-shift range of a polypeptide.

For sequential assignment, we employed triple-resonance experiments which establish correlations between the amide nitrogen and either its directly attached carbon neighbors or more distant carbons, in particular the C^{α} nucleus of the same or of the previous amino acid. Key features of these experiments were adiabaticity and band selectivity of the individual polarization-transfer steps in order to achieve a high sensitivity in selected spectral regions. Sequential assignment of all backbone resonances could be achieved by combining the information of two 2D correlation experiments.

A 3D variant of the band-selective, adiabatic triple-resonance experiments discussed was applied and should become particularly useful in larger molecules.

The fact that all spectra used for assignment are not very crowded shows that applications to larger peptides and proteins are possible. There, an optimum signal-to-noise ratio will become crucial and the efficiency of the polarization-transfer experiments will become a key requirement for these experiments. Some of the adiabatic transfer steps employed in this paper are already close to optimum; others can, hopefully, be further improved.

Acknowledgements

We thank Prof. B. Jaun (Organic Chemistry Laboratory, ETH Zürich) for recording a ^{13}C-TOCSY of a uniformly ^{13}C enriched antamanide sample dissolved in $CDCl_3$. Financial support by the Swiss National Science Foundation is acknowledged. A.D. was supported by a post-doctoral fellowship of the Max Planck Society, E.H. by a post-doctoral fellowship of the Deutsche Forschungsgemeinschaft.

References

Baldus, M. (1996) *Structural information from high-resolution solid-state NMR: Methodological improvements*, Ph.D. Thesis, ETH Zürich, Diss. No. 11847.

Baldus, M., Geurts, D.G., Hediger, S. and Meier, B.H. (1996) *J. Magn. Reson.*, **A118**, 140–144.

Baldus, M. and Meier, B.H. (1996) *J. Magn. Reson.*, **A121**, 65–69.

Baldus, M., Petkova, A.T., Herzfeld, J. and Griffin, R.G. (1998) *Mol. Phys.*, **95**, 1197–1207.

Bennett, A.E., Rienstra, C.M., Auger, M., Lakshmi, K.V. and Griffin, R.G. (1995) *J. Chem. Phys.*, **103**, 6951–6958.

Braunschweiler, L. and Ernst, R.R. (1983) *J. Magn. Reson.*, **53**, 512–528.

Bystrov, V.F. (1976) *Prog. NMR Spectrosc.*, **10**, 41–81.

Costa, P.R., Sun, B.Q. and Griffin, R.G. (1997) *J. Am. Chem. Soc.*, **119**, 10821–10830.

Ernst, M. (1993) *Untersuchungen zur Dynamik von Peptiden und Proteinen mit NMR-Relaxationsmethoden*, Ph.D. Thesis, ETH Zürich, Diss. No. 10390.

Fesik, S.W., Eaton, H.L., Olejniczak, E.T. and Zuiderweg, E.R.P. (1990) *J. Am. Chem. Soc.*, **112**, 886–888.

Garwood, M. and Ke, Y. (1991) *J. Magn. Reson.*, **94**, 511–525.

Griffin, R.G. (1998) *Nat. Struct. Biol.*, **5** (supplement), 508–512.

Grimmer, A.R., Kretschmer, A. and Cajipe, V.B. (1997) *Magn. Reson. Chem.*, **35**, 86–90.

Hardy, E.H., Verel, R. and Meier, B.H. (2001) *J. Magn. Reson.*, **148**, 459–464.

Hediger, S., Meier, B.H. and Ernst, R.R. (1995) *Chem. Phys. Lett.*, **240**, 449–456.

Hediger, S., Meier, B.H., Kurur, N.D., Bodenhausen, G. and Ernst, R.R. (1994) *Chem. Phys. Lett.*, **223**, 283–288.

Hohwy, M., Jakobsen, H.J., Eden, M., Levitt, M.H. and Nielsen, N.C. (1998) *J. Chem. Phys.*, **108**, 2686–2694.

Hong, M. (1999) *J. Biomol. NMR*, **15**, 1–14.

Hu, J.S. and Bax, A. (1997) *J. Am. Chem. Soc.*, **119**, 6360–6368.

Hwang, T., van Zijl, P.C.M. and Garwood, M. (1998) *J. Magn. Reson.*, **133**, 200–203.

Kao, L. and Barfield, M. (1985) *J. Am. Chem. Soc.*, **107**, 2323–2330.

Karle, I.L., Wieland, T., Schermer, D. and Ottenheym, H.C.J. (1979) *Proc. Natl. Acad. Sci. USA*, **76**, 1532–1536.

Kessler, H., Bats, J.W., Lautz, J. and Muller, A. (1989a) *Liebigs Ann. Chem.*, 913–928.

Kessler, H., Muller, A. and Pook, K.H. (1989b) *Liebigs Ann. Chem.*, 903–912.

Langer, B., Schnell, I., Spiess, H.W. and Grimmer, A.R. (1999) *J. Magn. Reson.*, **138**, 182–186.

Lee, M. and Goldburg, W.I. (1965) *Phys. Rev.*, **140**, A1261–1271.

Live, D.H., Davis, D.G., Agosta, W.C. and Cowburn, D. (1984) *J. Am. Chem. Soc.*, **106**, 1939–1943.

Marion, D. and Wüthrich, K. (1983) *Biochem. Biophys. Res. Commun.*, **113**, 967-974.

McDermott, A., Polenova, T., Bockmann, A., Zilm, K.W., Paulson, E.K., Martin, R.W. and Montelione, G.T. (2000) *J. Biomol. NMR*, **16**, 209–219.

Meier, B.H. and Earl, W.L. (1987) *J. Am. Chem. Soc.*, **109**, 7937–7942.

Nakai, T. and McDowell, C.A. (1992) *Mol. Phys.*, **77**, 569–584.

Pauli, J., Baldus, M., van Rossum, B., de Groot, H. and Oschkinat, H. (2001) *Chem. BioChem.*, **2**, 272–281.

Pauli, J., van Rossum, B., Forster, H., de Groot, H.J.M. and Oschkinat, H. (2000) *J. Magn. Reson.*, **143**, 411–416.

Rienstra, C.M., Hohwy, M., Hong, M. and Griffin, R.G. (2000) *J. Am. Chem. Soc.*, **122**, 10979–10990.

Sakakibara, S., Shimonishi, Y., Kishida, Y., Okada, M. and Sugihara, H. (1967) *Bull. Chem. Soc. Jpn.*, **40**, 2164–2167.

Schnolzer, M., Alewood, P., Jones, A., Alewood, D. and Kent, S.B. (1992) *Int. J. Pept. Protein Res.*, **40**, 180–193.

Sørensen, O.W. (1990) *J. Magn. Reson.*, **86**, 435–440.

Straus, S.K., Bremi, T. and Ernst, R.R. (1997) *J. Biomol. NMR*, **10**, 119–128.

Sun, B.Q., Rienstra, C.M., Costa, P.R., Williamson, J.R. and Griffin, R.G. (1997) *J. Am. Chem. Soc.*, **119**, 8540–8546.

Takegoshi, K., Nomura, K. and Terao, T. (1995) *Chem. Phys. Lett.*, **232**, 424–428.

Takegoshi, K., Nomura, K. and Terao, T. (1997) *J. Magn. Reson.*, **127**, 206–216.

Tycko, R. (1996) *J. Biomol. NMR*, **8**, 239–251.

Verel, R., Baldus, M., Ernst, M. and Meier, B.H. (1998) *Chem. Phys. Lett.*, **287**, 421–428.

Verel, R., Baldus, M., Nijman, M., Vanos, J.W.M. and Meier, B.H. (1997) *Chem. Phys. Lett.*, **280**, 31–39.

Verel, R., Ernst, M. and Meier, B.H. (2001) *J. Magn. Reson.*, **150**, 81–99.

Wieland, T. (1968) *Angew. Chem. Int. Ed. Engl.*, **7**, 204–208.

Wieland, T. and Faulstich, H. (1978) *Crit. Rev. Biochem.*, **5**, 185–260.

Zhang, S., Meier, B.H. and Ernst, R.R. (1994) *J. Magn. Reson.*, **A108**, 30–37.